Particle Size Distributions During and Performance of Preferential Crystallization of L-Asparagine·H_2O with Tailor-Made Additives

Peetikamol Kongsamai[1], Assistant Professor Chalongsri Flood[1], Professor Joop H. ter Horst[2], Professor Adrian E. Flood[3,*]

[1]School of Chemical Engineering, Suranaree University of Technology, 111 University Avenue, Nakhon Ratchasima, 30000, Thailand;

[2]EPSRC Centre for Innovative Manufacturing in Continuous Manufacturing and Crystallization (CMAC), Strathclyde Institute of Pharmacy and Biomedical Sciences, Technology and Innovation Centre, University of Strathclyde, 99 George Street, Glasgow G1 1RD, U.K.;

[3]Department of Chemical and Biomolecular Engineering, School of Energy Science and Engineering, Vidyasirimedhi Institute, 555 Moo 1, Payupnai, Wang Chan, Rayong 21210, Thailand;

*adrian.f.vistec@gmail.com

Preferential Crystallization (PC) is a process to separate enantiomers. We develop the efficiency of seeded, isothermal PC using tailor-made additives to inhibit the crystallization of the counter enantiomer. This research investigates inhibition of D-asparagine (D-Asn) monohydrate using D-glutamic acid (D-Glu) and D-aspartic acid (D-Asp) additives in PC by comparing the purity, yield and particle size distribution of the PC of L-Asn·H_2O from DL-Asn·H_2O. We use online measurement of the particle size distribution by FBRM and measurement of the product purity by HPLC. The amount of pure L-Asn·H_2O solid product that can be produced before crystallization of the counter enantiomer is higher when using the additives D-Asp and D-Glu. However, the crystal size of L-Asn·H_2O in PC without additives

increases faster than in PC with additives. This means that the additives inhibit not only the crystallization of D-Asn·H_2O but also the crystal growth of L-Asn·H_2O.

Keywords: Preferential crystallization, chiral separation, amino acids, additives, inhibition of crystallization

1. Introduction

Preferential crystallization (PC) is a process to separate the preferred enantiomer from a racemic mixture which contains an equal amount of the preferred enantiomer and the counter enantiomer, assuming the mixture crystallizes as a conglomerate forming system [1]. Recent reviews of PC include the following [2,3]. PC achieves separation in a single process step through seeding of the preferred enantiomer to a supersaturated racemic solution; the preferred enantiomer will crystallize at a higher rate than the counter enantiomer, and significant yield and enantiopurity can be achieved if the nucleation and growth of the counter enantiomer from the supersaturated solution can be avoided.

A major objective in the process is to prevent the spontaneous crystallization of the counter enantiomer. Many processes have been suggested to minimize or mitigate the effect of the crystallization of the counter enantiomer [4-10]. A recent review of stereoselective crystallization has given a useful overview of the topic, as well as a summary of useful methods [11]. One potentially useful idea is the use of tailor-made chiral additives, where a chiral additive can inhibit the crystallization of the enantiomorph having a similar chirality, generally known as the rule of reversal [12].

The aim of the current study is to determine whether the use of tailor made chiral additives can increase the time during which the preferred enantiomorph can be crystallized without crystallization of the counter enantiomorph, thus increasing the yield and enantiopurity of the crystal product in PC. Previously, we have studied the effect of additives to the solubility, metastable zone width, and growth rate in the PC process [13] but the effect

of the additives on the particle size distribution has not yet been studied. Therefore, this research studied the effect of D-Aspartic acid (D-Asp) and D-Glutamic acid (D-Glu) on the yield and particle size distribution in preferential crystallization of L-Asn·H_2O from DL-Asn·H_2O and also determined the crystal growth rate of L-Asn·H_2O in the PC experiments.

2. Experimental Methods

2.1 Materials

DL-asparagine monohydrate (DL-Asn·H_2O, 99+ wt%), and L-asparagine monohydrate (L-Asn·H_2O, 99+ wt%) were purchased from Sigma-Aldrich. D-aspartic acid (D-Asp, 99+wt%), and D-glutamic acid (D-Glu, 99+wt%) were purchased from ACROS. These reagents were used without further purification. Deionized water was used as the solvent.

2.2 Experimental Procedure

Seeded, isothermal PC experiments were performed with the following procedure. DL-Asn·H_2O solutions were prepared with the conditions shown in Tab. 1, in 300 g of water in a 500 mL crystallization vessel with a jacket to control the temperature. The solution was heated to 55°C to completely dissolve the crystalline material. Subsequently, the solution was cooled down with a cooling rate 1°C/min to the crystallization temperature at 20°C. The PC was seeded when the solution reached the crystallization temperature. The FBRM (Focused Beam Reflectance Measurement) probe was placed into the solution to measure the particle size distribution at 5 s intervals.

A sample of 5 mL of suspension was taken by syringe every 0.5 h to 1 h, and then filtered using a membrane filter. The solid product was kept in a desiccator for 1-2 days to completely dry crystal. The liquid and solid products were analysed for the enantiomeric excess (E) and yield (Y) of L-Asn·H_2O by HPLC. The purity of solid products was analysed by HPLC (1260 Infinity, Agilent Technologies) with a Chirobiotic T column. The HPLC

analysis was performed at 25°C using a 40:60 vol% ethanol: water mixture as a mobile phase with flow rate 0.25 mL/min and using UV detection at 210 nm. The injection volume was 5 μL. The retention times of L-Asn and D-Asn were 21.9 min and 25.8 min, respectively. The enantiomeric excess (*E*) and yield (*Y*) are defined by eq. (1) and (2) respectively.

$$E\ (\%) = \frac{C_L - C_D}{C_L + C_D} \times 100\% = \frac{A_L - A_D}{A_L + A_D} \times 100\% \qquad (1)$$

where C_L and C_D are the concentration of L-Asn·H_2O and D-Asn·H_2O in the solid product respectively. A_L and A_D are HPLC peak area of L-Asn·H_2O and D-Asn·H_2O in the solid product.

$$Y\ (\%) = \frac{m_t}{m_{th}} \times 100\% = \frac{m_p - m_s}{m_T - C \cdot V} \times 100\% \qquad (2)$$

where m_t is the mass of preferred enantiomer produced and m_{th} is maximum mass of the preferred enantiomer obtainable at equilibrium, which is determined by the total mass of the crystallizing species, m_T, minus the product of the solubility concentration, *C* (here in g/mL), and solution volume, *V*. Since a mass m_s of seed crystals is introduced at the start of the preferential crystallization resulting in a mass m_p of the preferred enantiomer product, the yield is further defined using $m_t = m_p - m_s$ in eq. 2. The additives used do not have a significant effect on the solubility of the solute at the concentrations they are added to the PC.

Table 1 The conditions for preferential crystallization of L-Asn·H_2O for finding the particle size distribution.

The FBRM determines the number of crystals passing the sensing zone within the time period of measurement (#/s), and hence the measurement needs calibration in order to calculate the total number of crystals per mass of solution (#/g). The particle count per g of solution was

calculated from a calibration based on standard suspensions using crystals that were sieved in the range between 75 and 90 μm; this range was consistent with the seed crystals used and the size of the crystals produced in the PC experiments, which were the result of the seed crystals and nuclei produced in the PC. Standards were produced with particle concentrations of 2, 4, 6, 8, and 10 g/L, and the chord length distribution (CLD) and particle counts were measured using the FBRM. The CLD of the calibration standards determined using the FBRM was slightly wider than the sieve range used, however this is typically found from sizing data as the sieving is not exact, and the chord length distribution here is not an exact representation of the crystal size distribution. The particle counts measured by FBRM was linearly correlated to the actual number of particles in the samples, with the correlation having r^2 = 0.9954. The correlation determined from this calibration is given as eq. (3). The Chord Length Distribution (CLD) from FBRM was calculated using icFBRM 4.3, the Mettler Toledo software packaged with the FBRM.

$$N / \#\cdot g^{-1} = 8.3016 \times N_{FBRM} \quad (3)$$

3. Results and Discussion

3.1 Preferential Crystallization Rate and Enantiomeric Excess

The results of the preferential crystallization of L-Asn·H_2O from DL-Asn·H_2O solutions, and from DL-Asn·H_2O solutions with D-Glu or D-Asp additives are shown in Fig. 1, with Fig 1a showing the time evolution of the L-Asn·H_2O concentration, and Fig 1b and 1c showing the time evolution of the amount of L-Asn·H_2O crystal and D-Asn·H_2O, respectively (using units of g crystal/g solution). The suspension density of L-Asn·H_2O has a finite value at the beginning of the PC due to the addition of the L-Asn·H_2O seed crystals. The crystallization for PC of L-Asn·H_2O from DL-Asn·H_2O solutions without additives is typical of PC processes, where the initial crystallization is mainly the preferred enantiomer, L-Asn·H_2O, but where the nucleation of the counter enantiomer occurs after a short period of

time which reduces the product enantiopurity. The rate of L-Asn·H_2O crystallization from the DL-Asn·H_2O solutions appears to decrease slightly when D-Glu and D-Asp additives are used, although the change is small compared to the experimental accuracy of the determination. A decrease in the rate of crystallization of L-Asn·H_2O could occur, because these D-amino acids additives decrease not only the crystal growth rate of D-Asn·H_2O but also decrease the crystal growth rate of L-Asn·H_2O, even though is a difference in the absolute configuration of the solute and the additive [13].

The concentration of D-Asn·H_2O from the preferential crystallization of L-Asn·H_2O in DL-Asn·H_2O with D-Glu and D-Asp additives is shown in Fig. 2. The D-Asn·H_2O concentration starts to decrease 3 h, 6 h, and 15 h from the start of the preferential crystallization of L-Asn·H_2O in DL-Asn·H_2O without additives, and with D-Glu and D-Asp additives respectively. The decrease in D-Asn·H_2O solute concentration is due to the D-Asn·H_2O crystallization. This shows that the additives effectively inhibit the crystallization of D-Asn·H_2O.

The amount of L-Asn·H_2O solid product in the preferential crystallization of L-Asn·H_2O in DL-Asn·H_2O increases with time (Fig. 1(b)) due to the preferential crystallization. The amount of L-Asn·H_2O solid product from crystallization in the absence of additives increases faster than it does in crystallizations in the presence of D-Glu or D-Asp additives. In Fig. 1(c), the amount of D-Asn·H_2O crystal product from DL-Asn·H_2O without additives increases faster than from DL-Asn·H_2O with D-Glu or (especially) D-Asp additives. In Fig. 2, the *E* of L-Asn·H_2O solid product decreased fastest when crystallized from DL-Asn·H_2O in the absence of additives, and the *E* of L-Asn·H_2O solid product decreases slowest when crystallized from DL-Asn·H_2O with D-Asp additive. These results also support the inhibition of D-Asn·H_2O through the use of D-Glu and D-Asp additives; the time available to produce product at 100 % *E* is increased when using the additives. The amount of L-Asn·H_2O solid product at a particular time decreases when using the additives, as shown in Fig. 1(b).

Fig. 3 shows how the enantiomeric excess of L-Asn·H_2O changes as the yield in the PC experiments increases. The maximum yield of L-Asn·H_2O for which product can be produced at 100 % *E* is 51% in PC from DL-Asn·H_2O solutions without additives, is 60% in PC from DL-Asn·H_2O with the additive D-Glu, and is 67% in PC from DL-Asn·H_2O with the additive D-Asp. Thus, the total yield of L-Asn·H_2O achievable at 100% *E* increases when using D-Glu and (especially) D-Asp additives.

Figure 1 (a) Solution phase concentration of L-Asn·H_2O in the preferential crystallization of L-Asn·H_2O in DL-Asn·H_2O with and without D-Glu and D-Asp additives; (b) suspension density of L-Asn·H_2O; (c) suspension density of D-Asn·H_2O.

Figure 2 (a) Solution concentration of D-Asn·H_2O in the preferential crystallization of L-Asn·H_2O in DL-Asn·H_2O with and without D-Glu and D-Asp additives; (b) Enantiomeric excess of L-Asn·H_2O in the preferential crystallization.

Figure 3 The relationship between *E* and *Y* of L-Asn·H_2O in the preferential crystallization of L-Asn·H_2O in DL-Asn·H_2O with and without D-Glu and D-Asp additives.

3.2 Chord Length Distribution During Preferential Crystallization

The chord length distribution (CLD) of the crystal product in the preferential crystallization of L-Asn·H_2O from DL-Asn·H_2O solutions with and without D-Glu and D-Asp additives is described in this section. This allows an analysis of the effect of additives to the CLD of the solid product (which contains both L- and D-Asn·H_2O in the period after the nucleation of the counter enantiomer). The CLD is significant in understanding mechanisms of the separation in the preferential crystallization, and the effect that the additives have on these mechanisms.

The CLD of the product crystals from the preferential crystallization of L-Asn·H_2O in DL-Asn·H_2O without additives is shown in Fig. 4. The x-axis is chord length, which is a measure of the crystal size, and the y-axis is the number-based population density of crystals using 1 g of solution as a basis. The total population density is corrected based on the calibration converting FBRM counts to numbers per g solution. The clear solution is the solution before seeding, 0 h refers to the seeding time, and 1 h to 7 h are the crystallization time in the preferential crystallization process. The solution before seeding has essentially no detectable particles. Seeds in the 150-180 μm size range were added at 0 h, after which the number of crystals increased rapidly with time due to secondary nucleation of the preferred enantiomer, causing the mode of the distribution to move to a smaller chord length, with a mode around 60 μm at 1 h. In the following time periods both the number of particles and the mode of the distribution increased with time. The mode of the final CLD is around 100 μm. The crystallization involved nucleation and growth of both D- and L-Asn·H_2O, however the CLD of this experiment shows only one peak. This is because the chord length distribution is wide. The CLD due to the nucleation of the D-Asn·H_2O, which begins significantly after the seeds of L-Asn·H_2O are added and occurs steadily over time rather than as a single burst, is hidden within the peak originally due to the seeding and nucleation of the L-Asn·H_2O.

In Fig. 4, the cumulative oversize distribution of crystal in the preferential crystallization is shown. The cumulative oversize distribution measures the total number of particles larger than a particular size using (in this case) a basis of 1 g of solution. At 0 h (at the seeding time), the median chord length which appears at half of the total number of crystals for that measurement, is highest because the L-Asn·H_2O crystal seed size is around 150-180 microns. After seeding the median crystal size is smaller because of the secondary nucleation of seed crystals. The chord length distribution, and cumulative oversize distribution during the preferential crystallization of L-Asn·H_2O in DL-Asn·H_2O with D-Glu additives are shown in Fig. 5, and in DL-Asn·H_2O with D-Asp additives in Fig. 6. The

benefits of using the cumulative oversize distribution rather than the number density distribution is that the change in the total number of crystals due to nucleation is more easily visualized as the increase in the cumulative oversize function at zero size (the value on the y-axis). In addition, the crystal growth rate of a set of particles can be easily visualized as the increase in the crystal size at a constant value of the cumulative number (a constant value on the y-axis). If all crystals in the suspension grow with approximately the same crystal growth rate, then the set of crystals at a particular value of the cumulative oversize will remain the same throughout the batch. This shows that by the end of the batch time used there is still a small level of supersaturation since the crystals continue to grow, although with a low rate, and there remains a small increase in the number of crystals in the batch.

Figure 4 The chord length distribution from the preferential crystallization of L-Asn·H_2O in DL-Asn·H_2O solution by FBRM. (a) CLD; (b) Cumulative CLD.

Figure 5 The chord length distribution from the preferential crystallization of L-Asn·H_2O in DL-Asn·H_2O solution with 5 mol% D-Glu additive. (a) CLD; (b) Cumulative CLD.

Figure 6 The cumulative oversize distribution of crystals in the preferential crystallization of L-Asn·H_2O in DL-Asn·H_2O solution with 5 mol% D-Asp additive. (a) CLD; (b) Cumulative CLD.

3.3 Crystal Growth Rate of L-Asn·H_2O during the Preferential Crystallization

It is possible to estimate the mean crystal growth rate of L-Asn·H_2O from the CLD presented in the previous section. The mean crystal growth rate was found based on the

time rate of increase in the size of the median sized crystals of L-Asn·H_2O at 1 h. These crystals were chosen because from 0 h to 1 h the crystal size significantly decreases because the secondary nucleation of L-Asn·H_2O seeds, and the average size of the seeds is uncertain because of the small numbers of seed. Basing growth rates on the cumulative number for the median crystal size at 1 h results in a more accurate measurement than if the median at 0 h is used.

The time dependence of the size of the median-sized crystals at 1 h is shown in Fig. 7. The crystal growth rate of L-Asn·H_2O is calculated from the rate of change of this crystal size with respect to time. The crystal growth rate of L-Asn·H_2O from preferential crystallization of L-Asn·H_2O in DL-Asn·H_2O with and without D-Glu and D-Asp additives is shown in Fig. 8. The crystal growth rate of L-Asn·H_2O from DL-Asn·H_2O with additives, particularly the D-Asp additive, is low when compared with the growth rate of L-Asn·H_2O from DL-Asn·H_2O solutions without additives because of the inhibition of D-Asp on the L-Asn·H_2O crystal. The rule of reversal [12] states that in the PC process, a chiral additive should inhibit the solute species having the same chirality, but in this case the additive also inhibits the enantiomorph of the opposite chirality. However, the D-Asp has a stronger inhibiting effect on the crystal growth of D-Asn·H_2O, as discussed in our previous study [13].

It is possible to calculate the time dependence of the relative supersaturation from Fig. 1(a), and the relationship between the crystal growth rate and time is given in Fig. 8. This allows determination of the relationship between the relative supersaturation and crystal growth rate, which is shown in Fig. 9. The growth rate of L-Asn·H_2O from DL-Asn·H_2O with D-Glu and D-Asp is very low when compared to DL-Asn·H_2O without any additives because of the inhibition of D-Glu and D-Asp on the crystal growth of L-Asn·H_2O. The inhibition due to D-Asp is stronger than the inhibition due to D-Glu, and this agrees with the result of our previous study which investigated the effect of these additives on the single crystal growth rates of L-Asn·H_2O [13].

The results in Fig. 9 were fitted with the crystal growth rate equation in eq. (3).

$$G = k_g \sigma^n \quad (3)$$

where G is the crystal growth rate, k_g is the growth rate constant, σ is relative supersaturation, and n is the growth rate order. The fitted parameters for this growth rate equation are shown in Tab. 3. The growth rate order, n, is approximately unity for the PC without additives, and higher than 1 in PC with additives.

Table 2 Mean crystal size of L-Asn·H_2O seed crystals in the preferential crystallization of L-Asn·H_2O in DL-Asn·H_2O from 1 h to 7 h.

Figure 7 The relationship between the crystal size and time of L-Asn·H_2O crystal in the preferential crystallization of L-Asn·H_2O in DL-Asn·H_2O with and without D-Glu and D-Asp additives.

Figure 8 The relationship between the crystal growth rate and time for L-Asn·H_2O crystal in the preferential crystallization of L-Asn·H_2O in DL-Asn·H_2O with and without D-Glu and D-Asp additives.

Figure 9 The relationship between the crystal growth rate and relative supersaturation of L-Asn·H_2O crystal in the preferential crystallization of L-Asn·H_2O in DL-Asn·H_2O with and without D-Glu and D-Asp additives.

Table 3 The fitting parameters of crystal growth rate of L-Asn·H_2O in preferential crystallization of L-Asn·H_2O in DL-Asn·H_2O with and without D-Glu and D-Asp additives.

The results of PC experiments to determine the time evolution of the enantiomeric excess and the yield, as well as *in-situ* measurements of the chord length distribution of crystals inside the PC lead to a consistent analysis of the effect of the tailor-made chiral additives to the PC of DL-Asn·H_2O. The additives delay the onset of crystallization of the counter enantiomer leading to an extended period during which the enantiopure product can be produced, and this allows for an increased yield of the enantiopure product in the PC. However, this benefit is slightly reduced, since the additives also decrease the growth rate of the preferred enantiomer. This causes the crystallization rate of the product being slowed, thus lowering the benefit caused by the use of additives. The net effect of the additives is still positive, although less so than if the additive did not also slightly inhibit the growth of the preferred enantiomorph.

Conclusions

The preferential crystallization L-Asn·H_2O from DL-Asn·H_2O with D-Asp and D-Glu additives increases the time of production of pure L-Asn·H_2O product and also the potential yield of the preferred enantiomorph as an enantiopure product. This occurs through an extension of the induction time for the counter enantiomer. Our previous study also shows that these additives inhibit crystal growth of the counter enantiomer, D-Asn·H_2O. However, the results of analysis of chord length distributions show that the additives D-Asp and D-Glu also inhibit the crystal growth rate of L-Asn·H_2O even though they are different to the solute in absolute configuration. This reduces the overall rate of crystallization of the preferred enantiomorph which limits the benefit of the effect of the additive. The overall effect of the additives on the achievable yield of the enantiopure product is still positive despite the limitation imposed by the reduced growth rate of the preferred enantiomer.

Symbols Used

Symbols

A	[-]	area of HPLC peak
C	[-]	concentration as g solute/g solution
G	[μm h^{-1}]	crystal growth rate
k_g	[μm h^{-1}]	crystal growth rate constant
m	[g]	mass
n	[-]	exponent in the crystal growth rate model
N	[# g^{-1}]	total number of crystals per g solution
N_{FBRM}	[# s^{-1}]	total number of counts per second measured by FBRM
V	[mL]	volume

Greek letters

σ	[-]	relative supersaturation

Sub- and Superscripts

D	D-enantiomorph
L	L-enantiomorph
p	preferred enantiomer product
s	seed crystals
th	theoretical at equilibrium

References

[1] J. Jacques, A. Collet, S. H. Wilen *Enantiomers, Racemates, and Resolutions*, J. Wiley & Sons, Inc., New York **1981**.

[2] G. Levilain, G. Coquerel, *CrystEngComm* **2010**, *12*, 1983-1992.

[3] C. Viedma, G. Coquerel, P. Cintas, in *Handbook of Crystal Growth*, 2nd ed., (Ed. T. Nishinaga) Elsevier, Amsterdam, The Netherlands **2015**, 951–1002.

[4] G. Levilain, M. J. Eicke, A. Seidel-Morgenstern, *Cryst. Growth Des.* **2012**, *12 (11)*, 5396–5401.

[5] K. Galan, M. J. Eicke, M. P. Elsner, H. Lorenz, A. Seidel-Morgenstern, *Cryst. Growth Des*. **2015**, *15 (4)*, 1808–1818.

[6] L. Gou, H. Lorenz, A. Seidel-Morgenstern, *Cryst. Growth Des*. **2012**, *12 (11)*, 5197–5202.

[7] A. Svang-Ariyaskul, W. J. Koros, R. W. Rousseau, Chem. Eng. Sci. **2012**, *77*, 35-41.

[8] S. Gonella, G. Levilain, G. Coquerel, *Therm. Anal. Calorim*. **2011**, *103*, 125–129.

[9] G. Levilain, C. Rougeot, F. Guillen, J.-C. Plaquevent, G. Coquerel, *Tetrahedron Asymmetr.* **2009**, *20 (24)*, 2769-2771.

[10] N. Wermester, O. Lambert, G Coquerel, *CrystEngComm*, **2008**, *10*, 724-733.

[11] A. A. Bredhikhin, Z. A. Bredikhina, *Chem. Eng. Technol.*, **2017**, *40 (7)*, 1211–1220.

[12] L. Addadi, S. Weinstein, E. Gati, I. Weissbuch, M. Lahav, *J. Am. Chem. Soc.*, **1982,** 104, 4610-4617.

[13] P. Kongsamai, A. Maneedaeng, C. Flood, J.H. ter Horst, A.E. Flood, *Eur. Phys. J. Spec. Top* **2017**., *226 (5),* 823-835.

Acknowledgements

The research was supported by the Thailand Research Fund (TRF) via the Royal Golden Jubilee Ph.D. program grant no. PHD/0097/2552, and Vidyasirimedhi Institute of Science and Technology. Instrumental support from the Frontier Research Centre at VISTEC is also acknowledged. JtH thanks the EPSRC Centre for Innovative Manufacturing in Continuous Manufacturing and Crystallisation (http://www.cmac.ac.uk) for support (EPSRC funding under grant reference: EP/I033459/1).

Figure 1 (a) Solution phase concentration of L-Asn·H_2O in the preferential crystallization of L-Asn·H_2O in DL-Asn·H_2O with and without D-Glu and D-Asp additives; (b) suspension density of L-Asn·H_2O; (c) suspension density of D-Asn·H_2O.

Figure 2 (a) Solution concentration of D-Asn·H_2O in the preferential crystallization of L-Asn·H_2O in DL-Asn·H_2O with and without D-Glu and D-Asp additives; (b) Enantiomeric excess of L-Asn·H_2O in the preferential crystallization.

Figure 3 The relationship between %*e.e.* and %Yield of L-Asn·H_2O in the preferential crystallization of L-Asn·H_2O in DL-Asn·H_2O with and without D-Glu and D-Asp additives.

Figure 4 The chord length distribution from the preferential crystallization of L-Asn·H_2O in DL-Asn·H_2O solution by FBRM. (a) CLD; (b) Cumulative CLD.

Figure 5 The chord length distribution from the preferential crystallization of L-Asn·H_2O in DL-Asn·H_2O solution with 5 mol% D-Glu additive. (a) CLD; (b) Cumulative CLD.

Figure 6 The cumulative oversize distribution of crystals in the preferential crystallization of L-Asn·H_2O in DL-Asn·H_2O solution with 5 mol% D-Asp additive. (a) CLD; (b) Cumulative CLD.

Figure 7 The relationship between the crystal size and time of L-Asn·H_2O crystal in the preferential crystallization of L-Asn·H_2O in DL-Asn·H_2O with and without D-Glu and D-Asp additives.

Figure 8 The relationship between the crystal growth rate and time for L-Asn·H_2O crystal in the preferential crystallization of L-Asn·H_2O in DL-Asn·H_2O with and without D-Glu and D-Asp additives.

Figure 9 The relationship between the crystal growth rate and relative supersaturation of L-Asn·H_2O crystal in the preferential crystallization of L-Asn·H_2O in DL-Asn·H_2O with and without D-Glu and D-Asp additives.

Table 1 The conditions for preferential crystallization of L-Asn·H_2O for finding the particle size distribution. The crystallization temperature is 20°C. The supersaturation ratio is calculated based on L-Asn·H_2O at 20°C. Additive contents are relative to DL-Asn·H_2O.

Condition	Supersaturation ratio of DL-Asn·H_2O	Additives	%additives
PC1	1.3	-	-
PC2	1.3	D-Glu	5%
PC3	1.3	D-Asp	5%

Table 2 Mean crystal size of L-Asn·H_2O seed crystals in the preferential crystallization of L-Asn·H_2O in DL-Asn·H_2O from 1 h to 7 h. The number mean crystal sizes are taken from the measured chord length distributions.

Time (h)	Mean crystal size (microns)
1	43.65
2	68.94
3	87.63
4	105.05
5	119.28
6	129.88
7	134.15

Table 3 The fitting parameters of crystal growth rate of L-Asn·H_2O in preferential crystallization of L-Asn·H_2O in DL-Asn·H_2O with and without D-Glu and D-Asp additives.

Preferential Crystallization in	k_g	n
DL-Asn·H_2O	145.0	1.02
DL-Asn·H_2O with D-Glu	248.8	1.70
DL-Asn·H_2O with D-Asp	2583.5	3.34

Table of Contents Entry

The efficiency of preferential crystallization can be increased by tailor-made additives. This work uses analysis of the amount, enantiopurity and size of the crystalline product to investigate the mechanisms involved. The additives inhibit the counter enantiomorph, and, to a smaller extent the preferred enantiomorph leading to improvement in the preferential crystallization.

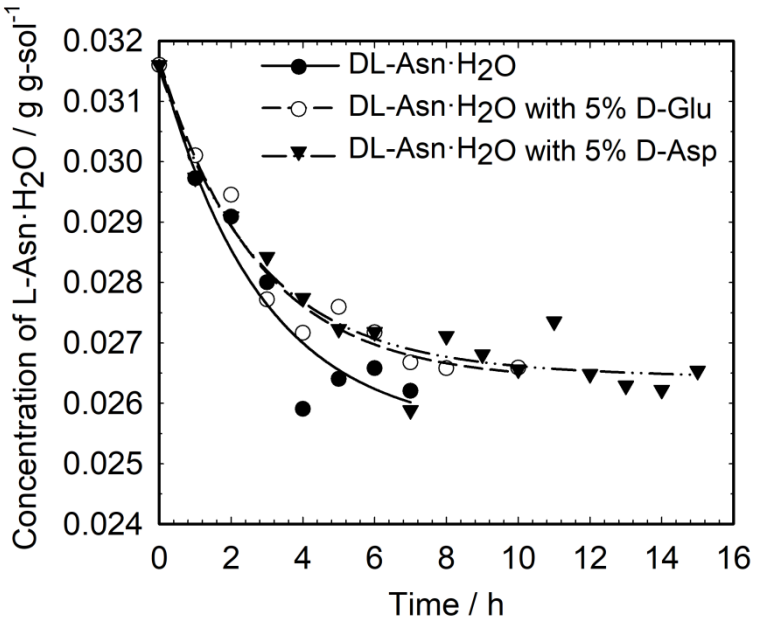
Concentration of L-Asn·H2O / g g-sol-1
0.032
0.031
0.030
0.029
0.028
0.027
0.026
0.025
0.024
0
2
4
6
8
10
12
14
16
Time / h
DL-Asn·H2O
DL-Asn·H2O with 5% D-Glu
DL-Asn·H2O with 5% D-Asp

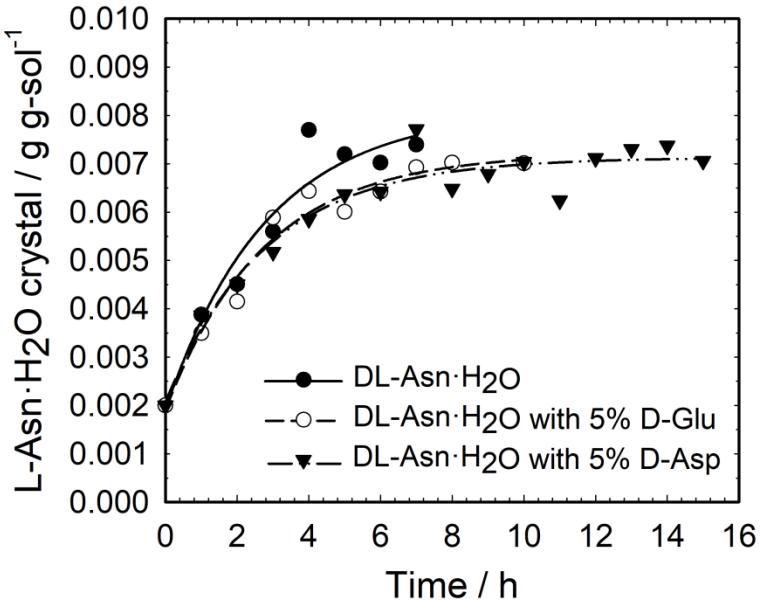
L-Asn·H2O crystal / g g-sol-1
0.010
0.009
0.008
0.007
0.006
0.005
0.004
0.003
0.002
0.001
0.000
0
2
4
6
8
10
12
14
16
Time / h
DL-Asn·H2O
DL-Asn·H2O with 5% D-Glu
DL-Asn·H2O with 5% D-Asp

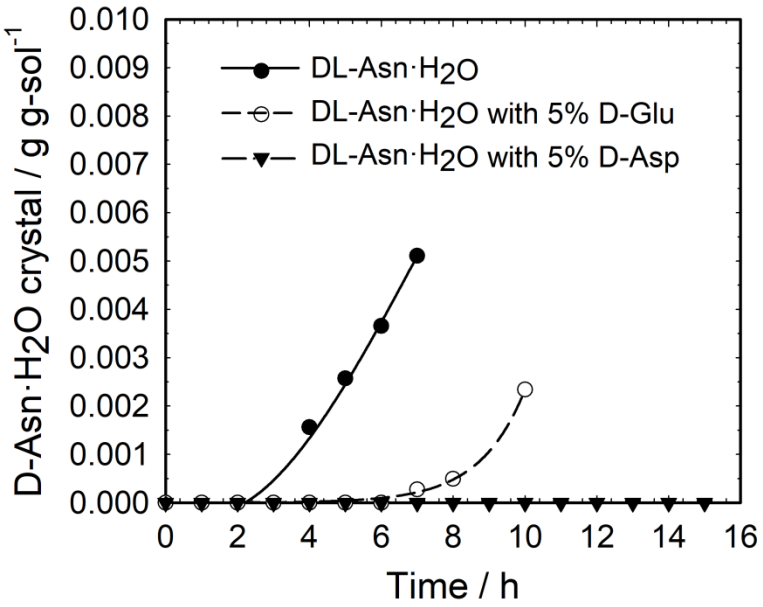
D-Asn·H2O crystal / g g-sol-1
0.010
0.009
0.008
0.007
0.006
0.005
0.004
0.003
0.002
0.001
0.000
0
2
4
6
8
10
12
14
16
Time / h
DL-Asn·H2O
DL-Asn·H2O with 5% D-Glu
DL-Asn·H2O with 5% D-Asp

Figure 1

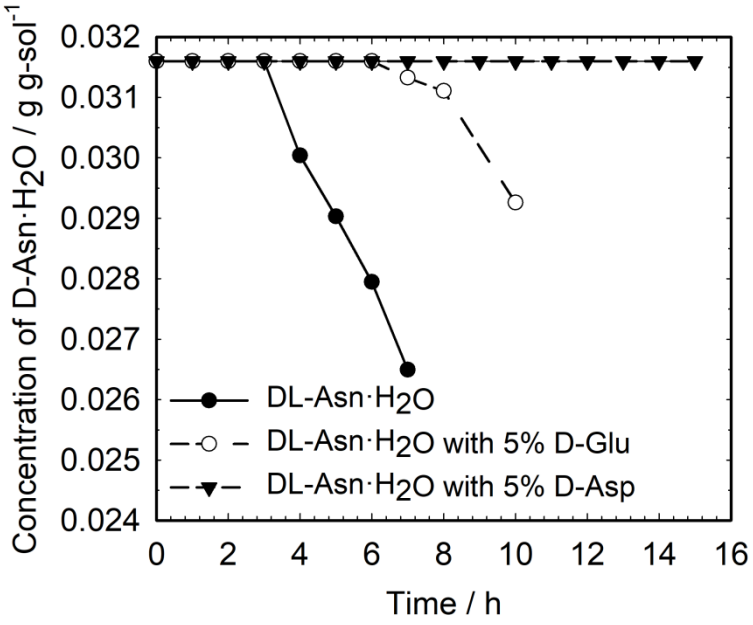
Concentration of D-Asn·H2O / g g-sol-1
0.032
0.031
0.030
0.029
0.028
0.027
0.026
0.025
0.024
0
2
4
6
8
10
12
14
16
Time / h
DL-Asn·H2O
DL-Asn·H2O with 5% D-Glu
DL-Asn·H2O with 5% D-Asp

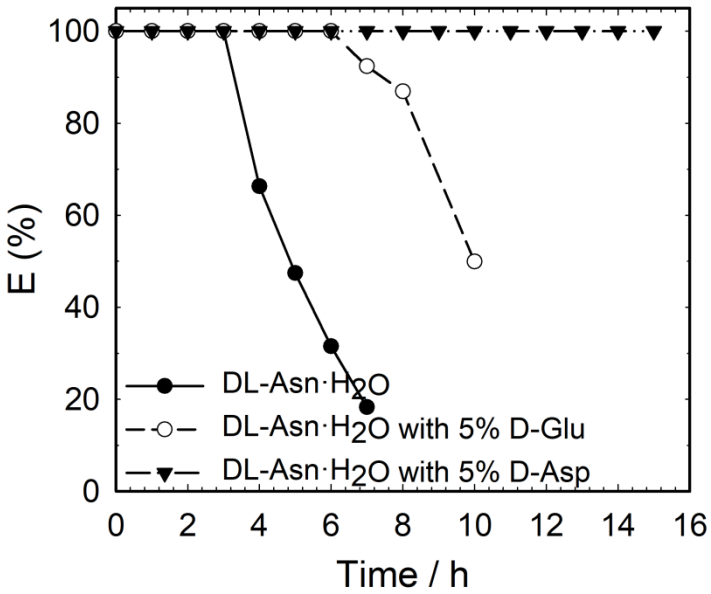
E (%)
100
80
60
40
20
0
0
2
4
6
8
10
12
14
16
Time / h
DL-Asn·H2O
DL-Asn·H2O with 5% D-Glu
DL-Asn·H2O with 5% D-Asp

Figure 2

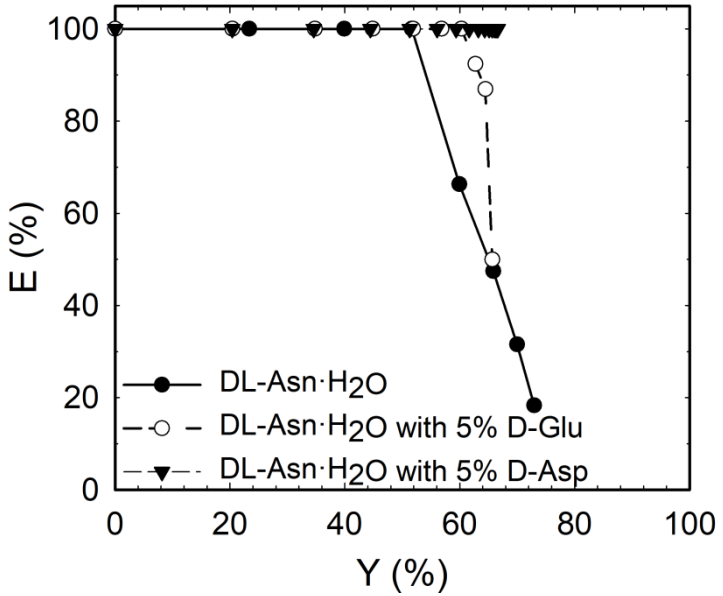
100
80
60
40
20
0
E (%)
0
20
40
60
80
100
Y (%)
DL-Asn·H2O
DL-Asn·H2O with 5% D-Glu
DL-Asn·H2O with 5% D-Asp

Figure 3

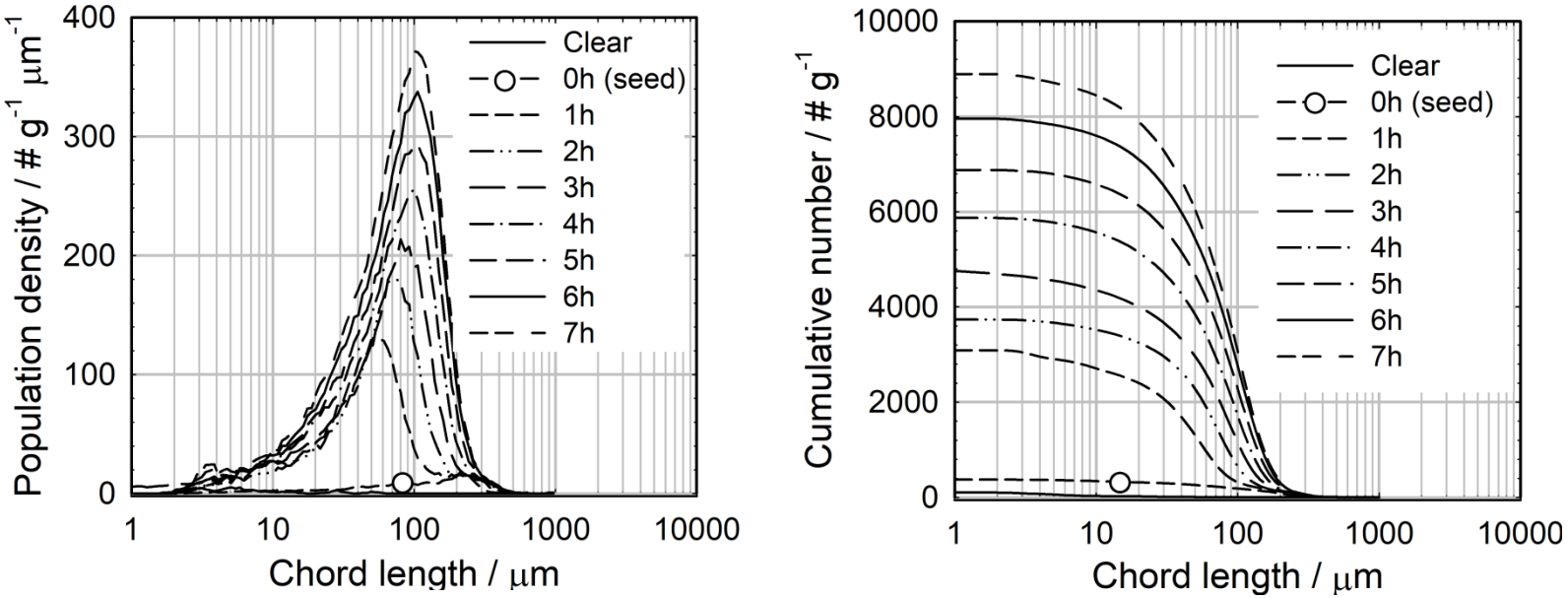
Population density / # g^{-1} μm^{-1}
400
300
200
100
0
1
10
100
1000
10000
Chord length / μm
Clear
0h (seed)
1h
2h
3h
4h
5h
6h
7h
Cumulative number / # g^{-1}
10000
8000
6000
4000
2000
0
1
10
100
1000
10000
Chord length / μm
Clear
0h (seed)
1h
2h
3h
4h
5h
6h
7h

Figure 4

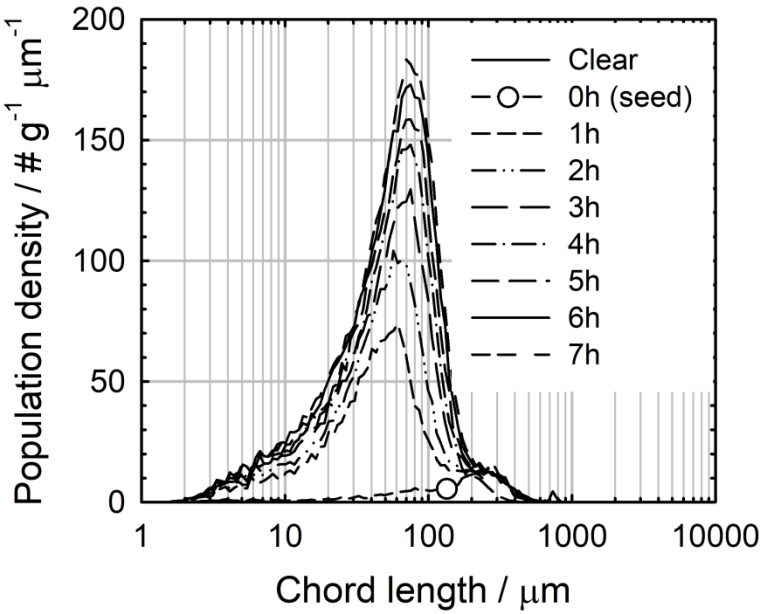
Population density / # g-1 μm-1
200
150
100
50
0
1
10
100
1000
10000
Chord length / μm
Clear
0h (seed)
1h
2h
3h
4h
5h
6h
7h

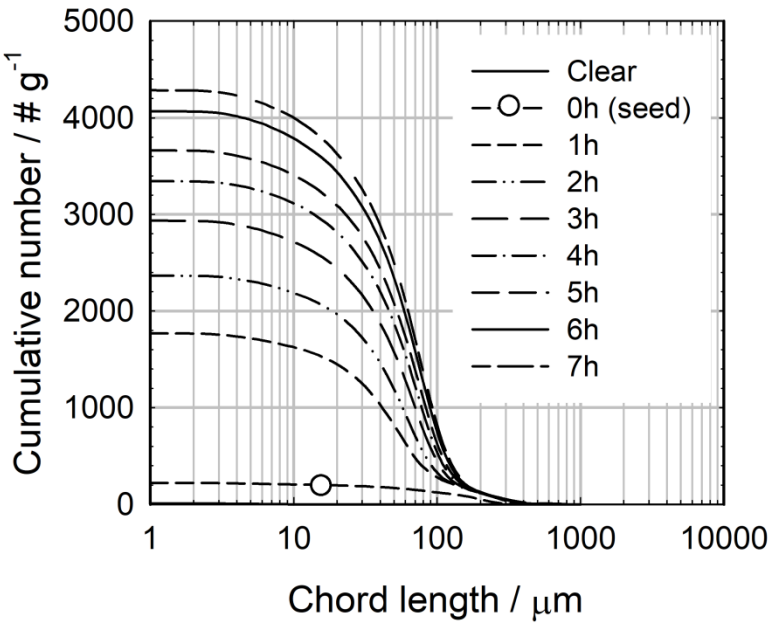
Cumulative number / # g-1
5000
4000
3000
2000
1000
0
1
10
100
1000
10000
Chord length / μm
Clear
0h (seed)
1h
2h
3h
4h
5h
6h
7h

Figure 5

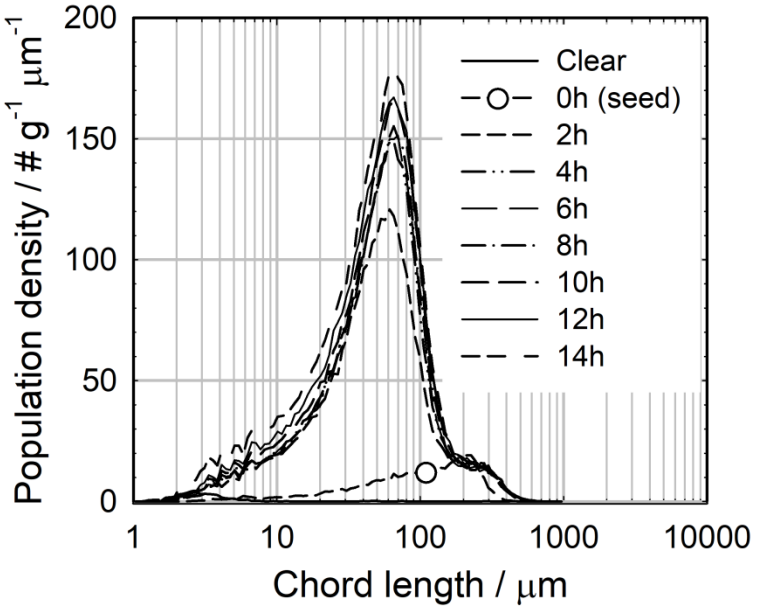
Population density / # g-1 µm-1
200
150
100
50
0
1
10
100
1000
10000
Chord length / µm
Clear
0h (seed)
2h
4h
6h
8h
10h
12h
14h

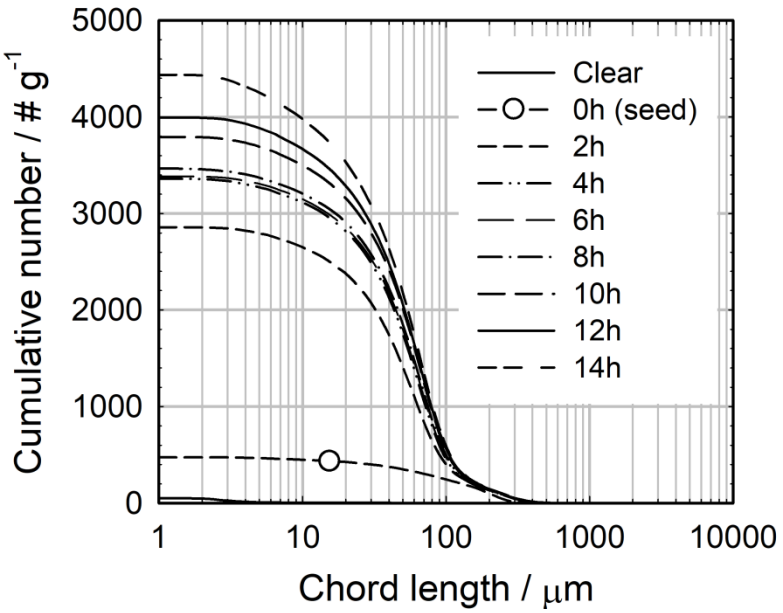
Cumulative number / # g-1
5000
4000
3000
2000
1000
0
1
10
100
1000
10000
Chord length / µm
Clear
0h (seed)
2h
4h
6h
8h
10h
12h
14h

Figure 6

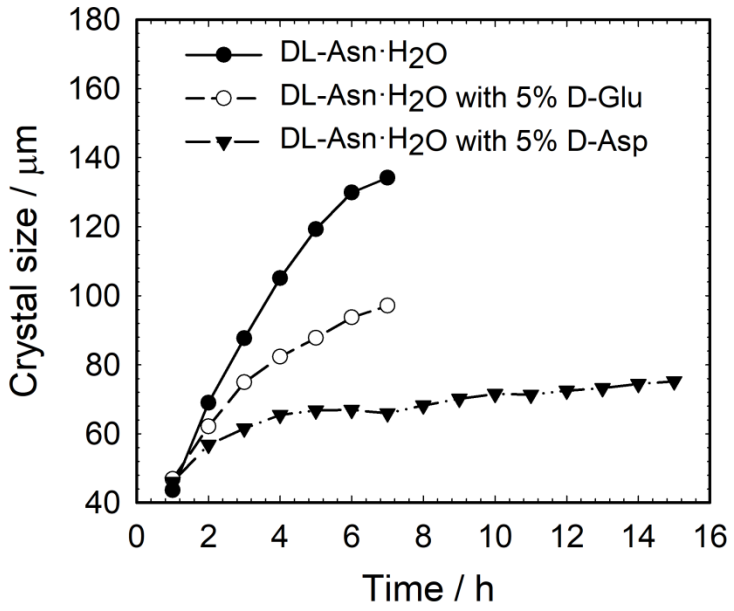
DL-Asn·H2O
DL-Asn·H2O with 5% D-Glu
DL-Asn·H2O with 5% D-Asp
Crystal size / μm
Time / h
180
160
140
120
100
80
60
40
0
2
4
6
8
10
12
14
16

Figure 7

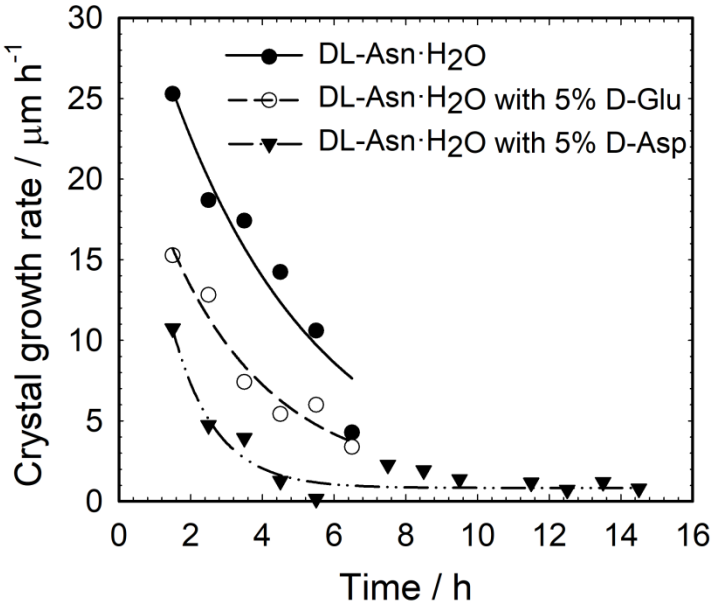
Crystal growth rate / μm h-1
Time / h
DL-Asn·H2O
DL-Asn·H2O with 5% D-Glu
DL-Asn·H2O with 5% D-Asp
0
5
10
15
20
25
30
0
2
4
6
8
10
12
14
16

Figure 8

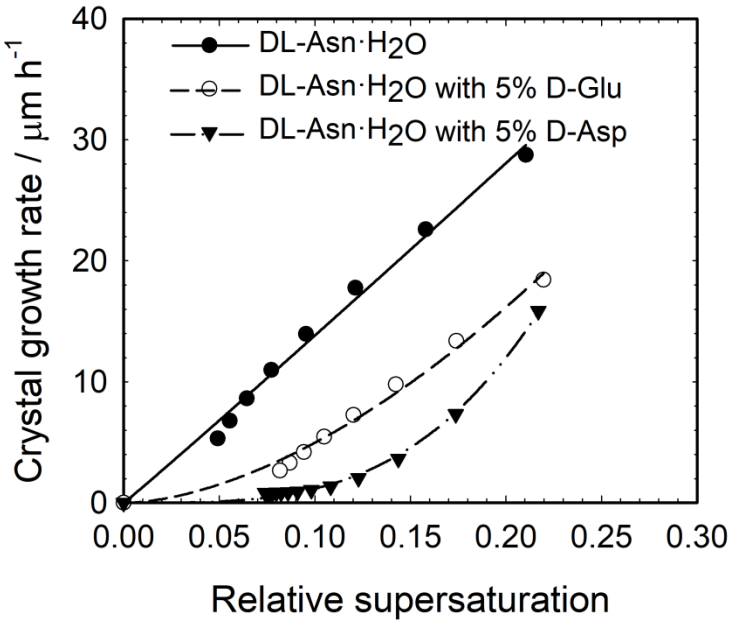
DL-Asn·H2O
DL-Asn·H2O with 5% D-Glu
DL-Asn·H2O with 5% D-Asp
Crystal growth rate / μm h-1
Relative supersaturation
0
10
20
30
40
0.00
0.05
0.10
0.15
0.20
0.25
0.30

Figure 9